ORIGINAL PAPER

Green synthesis of iron oxide nanoparticles for arsenic remediation in water and sludge utilization

Abhradeep Majumder[1] · Lata Ramrakhiani[2] · Debarati Mukherjee[2] · Umesh Mishra[1] · Avik Halder[3] · Ashish K. Mandal[3] · Sourja Ghosh[2]

Abstract

Iron oxide nanoparticles (IONPs) were synthesized via an affordable and environmentally friendly route using waste banana peel extract. The polyphenol-rich extract acted as a stabilizing and reducing agent resulting in formation of α-Fe_2O_3 with a particle size of around 60 nm. The composition, phase, morphology and size of the nanoparticles were analyzed by X-ray diffraction, field emission scanning electron microscopy, Fourier transform infrared spectroscopy, transmission electron microscopy and a Zetasizer. The efficiency of the IONPs was assessed in terms of arsenic(V) remediation from contaminated water within the range of 0.1–2.0 mg/L. Batch study showed that IONPs had a high As(V) adsorption capacity of about 2.715 mg/g at 40 °C. A statistical approach, viz. an artificial neural network, was adapted for modeling and optimization of the process parameters for achieving maximum As(V) removal efficiency. A set of 54 experimental sets were conducted and the predicted model generated showed an R^2 value of 0.9971 and the corresponding mean squared error value was 0.0000601. Surface binding of the As(V) phenomenon on the green synthesized IONPs was explained on the basis of FTIR spectroscopy, X-ray photoelectron spectroscopy, X-ray fluorescence spectroscopy of the control and the As(V)-loaded IONPs. The spent adsorbent was successfully immobilized in phosphate glass matrix with an objective to provide a complete and sustainable solution for arsenic contamination.

✉ Sourja Ghosh
sourja@cgcri.res.in; sourja.g@gmail.com
http://www.cgcri.res.in

1   Department of Civil Engineering, National Institute of Technology, Agartala, Tripura 799 055, India

2   Ceramic Membrane Division, CSIR-Central Glass and Ceramic Research Institute, 196, Raja S.C. Mullick Road, Kolkata 700 032, India

3   Glass Division, CSIR-Central Glass and Ceramic Research Institute, 196, Raja S.C. Mullick Road, Kolkata 700 032, India

Graphical abstract
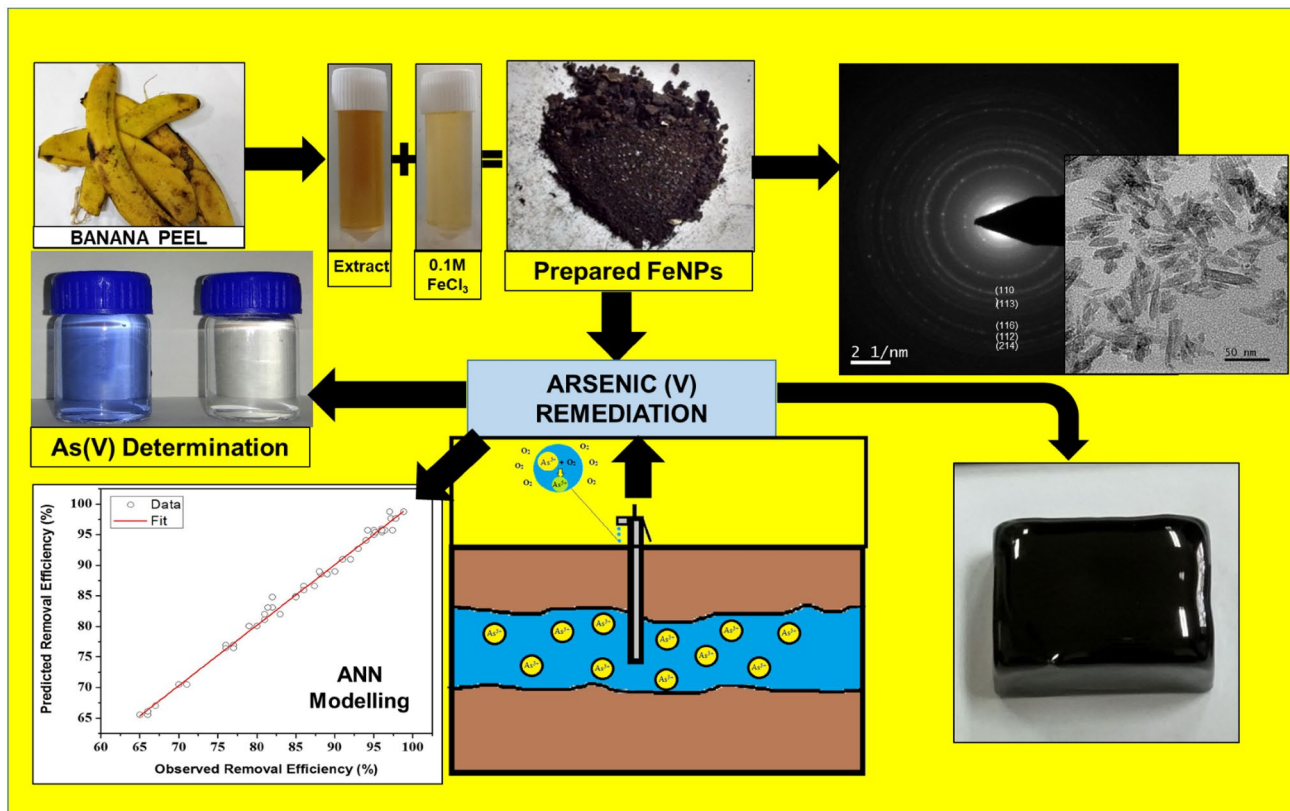
Introduction

The presence of arsenic as a toxic contaminant in water, especially groundwater, has led to health hazards and suffering of people and has become a pivotal water quality problem across the globe. Arsenic usually occurs in groundwater due to natural weathering of arsenic-containing rocks, minerals ores, and volcanic activities. In addition, anthropogenic activities also contribute to its release to the environment such as agriculture, wood preservation, electronics, metallurgy, and medicine. Moreover, an abundance of As-bearing minerals present in weathered rocks and soils of the Earth's crust are slowly entering into groundwater and thereby increasing the pollution and toxicity in places with no background of arsenic-related health problems. The most arsenic-affected countries reported are Bangladesh, India, China, Argentina, Mexico, Japan, Hungary, Romania, Taiwan, Chile, Vietnam and many parts of the USA. In India, the states of West Bengal, Tripura, Manipur, Uttar Pradesh, and Bihar have reported high levels of arsenic (Bundschuh and

Maity 2015; Chakraborti et al. 2016). Drinking arsenic-rich water over a long period has become unsafe, as arsenic has been documented as a carcinogen. Skin cancer and internal cancer have been commonly reported and other symptoms of chronic arsenic poisoning include keratosis, loss of pigmentation, and hyperpigmentation. According to the World Health Organization (WHO), the present guideline value of arsenic in groundwater is 0.01 mg/L. However, many countries are still adhering to the standard permissible limit of 0.05 mg/L of arsenic (Mohan and Pittman 2007).

The arsenic species present in natural water are hydrated anions of As(V), i.e. arsenate ($H_2AsO_4^-$) and arsenite ($HAsO_4^{2-}$), and the hydrated As(III), the neutral H_3AsO_3 molecule. Arsenic-related diseases have no known specific and/or effective medical treatment, but consuming arsenic-free water can help arsenic-affected people sred the symptoms of arsenic toxicity. Hence, provision for arsenic-free water is urgently required to alleviate arsenic toxicity and protection of health and well-being of people living in acute arsenic-affected areas.

Traditional applied technologies for arsenic removal include lime treatment, co-precipitation, coagulation and flocculation, oxidation, anion exchange or chelation, membrane techniques, and adsorption by activated carbon. However, these techniques have limitations like ineffective removal for low concentrations, high capital, and operational cost and the safe disposal of the residual metal/arsenic sludge (Fierro et al. 2009; Mandal et al. 2015). Among the possible treatment processes, adsorption has attained immense interest for its easy operation, high-efficiency characteristic, safe handling as compared with the contaminated sludge produced by precipitation, and having more versatility than ion exchange. The effectiveness of adsorption-based techniques depends primarily on the type of adsorbent used. A number of adsorbents have been reported for arsenic removal, such as activated carbon, waste biological materials, mineral oxides and polymer resins (Chiban et al. 2012). Moreover, there are numerous reports on the good adsorption capacity of iron oxide materials such as goethite (R-FeOOH), hematite, amorphous hydrous ferric oxide, crystalline ferric oxide (ferrihydrite), limonite, magnetite and iron-containing granular activated carbon for removal of both As(V) and As(III) from aqueous solutions (Zhimang Gu and Deng 2005; Gallegos-Garcia et al. 2012). However, literatures on several adsorbents have shown that arsenic removal cannot be achieved up to the permissible limits of drinking water. Furthermore, the adsorption process still has certain limitations as it could not achieve a breakthrough progress at commercial levels, probably due to the lack of appropriate adsorbents with effective adsorption capacities and commercial-scale setups (Brunson and Sabatini 2009). Therefore, the search for suitable method(s) of stable and long-serving arsenic remediation is essential.

Currently, water and wastewater treatment by adsorption using nanoparticles (NPs) as adsorbents have been an area of focus due to NP's extremely small size and large surface-to-volume ratio, and they exhibit novel characteristics compared to the large particles of bulk material (Ali 2012). The physical and chemical protocols of NP synthesis require extensive care and use highly expensive chemicals that are hazardous to the environment and may pose health risks. Iron NPs specifically have a significant advantage for arsenic adsorption because they have a net positive charge while arsenic(V) in water is negatively charged which can accelerate the adsorption process (Mohan and Pittman 2007). Iron oxide NPs (IONPs) have been synthesized using chemicals like $NaBH_4$ and $LiBH_4$ as reducing agents which produce byproducts which have detrimental effects on the environment. Some of the chemical reagents are flammable, toxic and expensive and the process involves a high amount of energy consumption. Hence, a cost-efficient, socially acceptable and eco-friendly adsorbent is required that can efficiently remove arsenic from groundwater while reducing

the concentrations to below permissible limits and making it safer for drinking and agriculture. The biological method of synthesis using extracts from plant parts and/or agricultural waste is an eco-friendly, benign, clean and low-cost alternative method, which reduces the metal ions in a shorter time as compared to microbes (Herlekar et al. 2014).

In the present study, biologically synthesized IONPs have been preferred over other low-cost, waste-derived adsorbents for arsenic(VI) adsorption from contaminated groundwater. Application of various plant extracts has been reported for green synthesis of IONPs (Herlekar et al. 2014). The presence of polyphenols, glutathione, alkaloids, polysaccharides, and other alcoholic compounds present in plant extracts not only help in the reduction of metal ions to stable NPs but also gives stability to the NPs (Mukherjee et al. 2016). IONPs have been synthesized using aloe vera leaf extract. The major drawbacks of using aloe vera plant leaf resource for NP synthesis lead to the destruction of plants. Use of banana peel, an agro-waste, could be a source of low-cost reducing agents, and provides a possible way to avoid destruction of plants and to serve the additional purpose of pollution mitigation.

Proper management of the arsenic-rich adsorbent could be the need of the hour. Conventionally, the management of produced spent biosorbent followed by dumping in landfills, storage or incineration will eventually lead to groundwater contamination. Some of the innovative suggestions reported in the scientific literature include formation of bricks, tiles, cement and concrete materials for inertization of hazardous substances. However, these sludge management processes have not satisfied the toxicity characteristic leaching procedure (TCLP) tests and have showed unpredictable leaching for longer period of times (Weng et al. 2003). In this work, the inertization of hazardous arsenic-laden biosorbent was studied in a phosphate glass matrix. Iron phosphate glasses are known to have low melting temperatures, high thermal and mechanical stability, chemical durability, and slow dissolution rates in water. It can incorporate high concentrations of the waste components, and reduce the volume and cost of the prepared glass for various applications. The glasses have been investigated as a viable technological alternative for effective management of spent fuel and radioactive waste (Mishra et al. 2013; Mandal et al. 2015).

The aim of the study was to reduce the As(V) concentration in groundwater to below the permissible limit using green synthesized IONPs as the adsorbent. Banana peel extract was used as the reducing agent for reduction of $FeCl_3$ to IONPs. The prepared adsorbent, i.e. IONPs, was characterized using X-ray diffraction (XRD), transmission electron microscopy (TEM), Zetasizer analysis, and Brunauer–Emmett–Teller (BET) surface area analysis. Arsenic(VI) adsorption was carried out using batch adsorption experiments in synthetic medium and was characterized

using X-ray fluorescence (XRF), Fourier transform infrared (FTIR) spectroscopy, X-ray photoelectron spectroscopy (XPS) and field emission scanning electron microscopy/energy-dispersive X-ray (FESEM-EDX) analysis techniques. The arsenic-loaded sludge was finally incorporated into phosphate glass matrix and confirmed by XRD analysis for effective sludge utilization and safe disposal to the environment.

Materials and methods

Synthesis and characterization of nanoparticles

The biological synthesis of IONPs was carried out using waste banana peel extract and anhydrous $FeCl_3$ (Merck, Germany, AR grade) as the initial precursor (Mukherjee et al. 2016). Banana peels were chosen because they are rich in various phenolic compounds and antioxidants. They have higher reducing ability compared to other fruit peels and were reported to have high ferric reducing ability (Ibrahim 2015; Vu et al. 2018). The waste banana peels collected from kitchen waste were thoroughly washed and oven-dried at 100 °C for 3–4 h for complete removal of moisture giving them a black and brittle texture. These were crushed and ground to powder form and were boiled in distilled water for about 30 min for the preparation of brown-colored, polyphenol-rich banana peel extract. The peel extract thus formed was added to $FeCl_3$ solution (0.1 M) in 1:1 ratio (v/v). The mixture was subjected to continuous heating at 80 °C and stirring (500 rpm) until the color changes from yellowish to black indicated the formation of IONPs. The solution was oven-dried to separate the formed NPs from the solution. The NPs were washed twice with distilled water and centrifuged to remove the reaction impurities. The NPs thus obtained were dried at 100 °C in an oven and stored in a desiccator for further use.

The synthesized IONPs were characterized in terms of XRD using a Philips 1710 diffractometer to predict the crystallinity and phase of the synthesized IONPs. Cu ($\alpha = 1.541 A°$ at 25 °C) was used as the anode material and the range of scan was from $2\theta = 20.02°$ to $2\theta = 79.97°$. The crystallite size was calculated using Scherrer's formula $D = k\lambda/\beta \cos\theta$, where k is a constant with value of 0.9–1.0, λ is the X-ray wavelength, β is the full-width half maxima and θ is the Bragg's angle. FESEM (Zeiss, Germany) was used to study the microstructure and morphology of the synthesized IONPs before and after As(V) adsorption. The elemental compositions were established by EDX. TEM (Tenchai G2, 30ST, FEL, USA) analysis was done to confirm the morphology and the particle size of the IONPs. Also conducted were BET surface area, zetasizer and zeta potential analysis. The BET method was used to determine the specific surface area of the NPs using a Quantachrome Autosorb Automated Gas Sorption System (USA). The particle size and zeta potential (zetasizer, nanoseries, Malvern) of the synthesized IONPs were also determined. The adsorbent was dispersed in distilled water and sonicated for 30 min to get rid of any agglomeration. The particle size measurement is based on the dynamic light scattering (DLS) method. The particle size was estimated by measuring their Brownian motion. Zeta potential of the particles was analyzed to find the net charge on the particles when dispersed in water. The presence of different functional groups and chemical bonds in the synthesized IONPs and arsenic-loaded adsorbent were identified within the range of 400–4500 cm^{-1} using FTIR spectroscopy (PerkinElmer, USA). For FTIR study, all the adsorbent samples were pressed into spectroscopic-quality KBr (potassium bromide) translucent pellet with a sample-to-KBr ratio of about 1:100. XPS measurements were carried out for the prepared IONPs (control adsorbent) and As(V)-loaded IONP samples using a PHI 5000 Versaprobe-II XPS analyzer (USA). The Mg-Kα source (1253.6 eV) and a hemispherical analyzer with 16-channel detector was located at a 54.7°position with respect to the sample surface (analyzer axis) and run at 300 W (10 keV and 30 mA) with a pressure of 5×10^{-8} torr inside the vacuum chamber. The spectra were obtained using a Versaprobe-IV lens system scanned from ~ 1-0 to 720-μm diameter and recorded via SmartSoft Versaprobe 2.4.0.9 software. These spectra were fitted to a Gaussian–Lorentzian distribution using Origin 8.5 software to determine the core-level binding energy of the Fe2p, As3d, C1s, O1s, and N1s elements. For elemental analysis of the IONP samples in solid phase before and after As(V) sorption, XRF was performed using an XRF spectrometer (Axios, PANalytical, The Netherlands).

Arsenic(V) adsorption studies

Batch adsorption experiments were executed in various dilutions of commercially available standard As(V) solution (1000 mg/L; Merck, India) using synthesized IONPs as adsorbent. Influence of various adsorption parameters viz. effects of temperature (20–40 °C), pH (2–10), adsorbent dose (0.5–4 g/L,) and initial As(V) concentration (0.1–2.0 mg/L) on As(V) removal using IONPs were studied. The solutions were stirred at 300 rpm for 8 h to achieve maximum As(V) adsorption. The solutions were then filtered using 0.2-μm polyvinylidene fluoride (PVDF) disposable syringe filters. As(V) concentrations was determined by colorimetric method at a wavelength of 862 nm (ZEN 2600 UV–visible spectrophotometer, Varian, Australia), per Dhar et al. (2004). The amount of arsenic(V) adsorbed and the arsenic adsorption capacity (q_e) of IONP was given according to Eqs. 1 and 2, respectively.

$$\text{Adsorption } (\%) = (C_i - C_e)/C_i \times 100 \tag{1}$$

$$q_e = V(C_0 - C_e)/m \tag{2}$$

where C_i is the initial As(V) concentration (mg/L), C_e is the As(V) concentration after adsorption, m is the dosage of IONPs (g), and V is the volume of As(V) solution (mL).

Artificial neural network modeling

An artificial neural network (ANN) is nonlinear model. It is much easier to comprehend and use as compared to other statistical methods. ANNs with a back-propagation (BP) learning algorithm is widely used in solving various modeling problems. The tool has been used to map large datasets and has been successfully applied for modeling of various adsorption processes. The predicted values from an ANN model have far more accurate results compared to other models (Debnath et al. 2016b). The main idea of ANNs has been adopted from that of the neural cells present in the brain. The computational system is inspired by the structure, processing method, and the learning ability of the brain. It is composed of a large number of neurons and weighted connections. An ANN is chosen mainly because of its massive parallelism, learning and generalization ability, and fault tolerance. It learns by taking an example and creating a set of connection weights which are again implemented on another similar kind of example.

The influence of the four influencing, independent parameters viz. pH, adsorbent dosage, temperature, and initial concentration on removal of As(V) was studied using the ANN tool. A three-layer, feed-forward back-propagation network was adapted for our purpose. The back-propagation is used to compute the gradient nonlinear multiple networks. A vast amount of input and output data can be stored in back-propagation and no definite mathematical equation is required to describe the mapping for performing the modeling (Ghosal and Gupta 2017). A tan-sigmoid transfer [Eq. (3)] function was used at the hidden layer and a linear (purelin) transfer function [Eq. (4)] was used at the output layer (Debnath et al. 2016a, b).

$$\tan \text{sig}(\text{sum}) = \frac{1 - \exp(-\text{sum})}{1 + \exp(-\text{sum})} \tag{3}$$

$$\text{Purelin}(\text{sum}) = \text{sum} \tag{4}$$

A single hidden layer was used for the study and the number of neurons was varied from 1 to 30. The Levenberg–Marquardt (LM) feed-forward back-propagation algorithm with 1000 epochs was selected for training the networks. The choice of training algorithm mainly depends on the complexity of the problem, and the LM algorithm is the most commonly used training algorithm. The LM algorithm is used for nonlinear curve fitting of a set of independent and dependent variables and obtaining parameters of the model curve so that there is minimum standard deviation (SD; Ghosal and Gupta 2016). The optimum number of nodes in the hidden layer lies between $2n + 1$ (Debnath et al. 2016a, b). In this study, a trial-and-error method was implemented to select the number of nodes by varying the number of nodes from 1 to 30. The performance of the ANN model was analyzed according to the determination coefficient (R^2) transfer [Eq. (5)] and mean squared error (MSE) transfer [Eq. (6)].

$$\text{MSE} = I/N \sum_{i=1}^{N} \left(\left| y_{\text{prd},i} - y_{\text{exp},i} \right| \right)^2 \tag{5}$$

$$R^2 = 1 - \frac{\left[\sum_{i=1}^{N} (y_{\text{prd},i} - y_{\text{exp},i}) \right]}{\left[\sum_{i=1}^{N} (y_{\text{prd},i} - y_m) \right]} \tag{6}$$

where N is the number of data sets, $y_{\text{prd},i}$ is the model-predicted value, $y_{\text{exp},i}$ is the experimental value, and y_m is the arithmetic mean of the experimental data sets.

A face-centered central composite design (CCD) was used to generate the 54 experimental data sets. The number of replicates of factorial points, axial (star) points, and center points were 2, 2, and 6, respectively, with the value of alpha being 1. 80% of the data points was used for training, 10% of the data was used for testing the remaining, and 10% was used for validating purposes. The adsorption parameters, pH (2–10), adsorbent dose (0.5–4 g/L), temperature (20–40 °C), and initial concentration (0.1–2 mg/L) were used as input parameters, and the percentage removal for each set of experimental data points was taken as the output. The experimental design comprising 54 data sets are given in Table S1. To avoid numerical overflow, all the input and the output data were normalized between 0 and 1 using the following expression [Eq. (7)].

$$X_{\text{norm}} = \frac{X - X_{\min}}{X_{\max} - X_{\min}} \tag{7}$$

where X_{norm} is the normalized value, $X_{\max}$ and $X_{\min}$ are the maximum and minimum value of the data sets, respectively.

As(V) removal from a contaminated groundwater system.

Adsorption experiments in groundwater

Arsenic-contaminated groundwater sample was collected from Akrampur, Barasat in the Hooghly district of West Bengal, India. The water was subjected to batch-mode

As(V) adsorption using synthesized NPs at the optimized experimental conditions (pH = 6, temperature = 40 °C, IONP adsorbent dose = 2 g/L) for 2 h at a stirring of 300 rpm. The groundwater samples were characterized in terms of the cations and anions present in the raw and post-treated water using an ion chromatography (IC) method (Metrohm, Switzerland). As(V) concentrations were analyzed as described earlier.

Safe disposal of exhaust adsorbent: incorporation in glass matrix

In the present study, the safe disposal of generated arsenic-contaminated IONPs, i.e. spent adsorbent as phosphate glass formulations, to the environment is recommended with a productive manner for possible utilization in new products. The feasibility study was carried out by incorporating various concentrations of the spent adsorbent into the phosphate glass matrix. The glassy phase of prepared glass was confirmed by XRD characterizations. The prepared glass was further tested for leaching of the incorporated metal for a period of 28 days. The detail study is described in following steps.

The spent adsorbent was dried at 100 °C for 6 h to remove any moisture content. The glass batches were prepared by mixing a defined amount of phosphate base glass matrix with 15% and 20% of the spent adsorbent. The mixtures were placed in an alumina crucible (30 mL) and melted at 1300 °C in a resistive heating furnace (bottom loading-raising hearth furnace, Deltech model DT-31-BL-810-KC-E3504) for 30 min. The molten glass was transferred to a preheated stainless steel mold. The process was followed by annealing in a muffle furnace at 360 °C for 2 h and subsequently controlled cooling to room temperature to eliminate any thermal stress (Ramrakhiani et al. 2017).

XRD analysis was used to study the crystalline and noncrystalline phases of the prepared glass. The starting position was $2\theta = 10°$ and the end position was $2\theta = 90°$ with a step size of $2\theta = 0.05°$. Cu was used as the anode material having $\alpha = 1.541A°$ at 25 °C.

The prepared glass samples were subjected to leaching test for a continuous 28 days by dissolution experiments using deionized water heated at 75 °C for 6 h per day. The standard practice of determining the chemical durability of glass samples was conducted based on the dissolution rate (DR) in deionized water at various temperatures like 50, 75, and 95 °C (Hémono et al. 2010; Chenu et al. 2010; Ramrakhiani et al. 2017). The DR was calculated using the following equation:

$$DR = \frac{\Delta m}{St} \tag{8}$$

where Δm is the weight loss (g), S is the total sample surface area (cm^2), and t is the immersion time (min).

First of all, the glass samples were cut into small blocks, polished, and weighed (Mettler Toledo ± 0.00001 g). The surface area and dimensions of the prepared glass were measured with a micrometer digital Vernier caliper. This was followed by hanging the glass blocks in deionized water at 75 °C for 6 h with intermittent shaking for 5 min (3 times a day). The DRs were studied for a 28-day thermal cycle and samples were collected at every 7-day interval. The release of metal ions was determined by inductively coupled plasma (ICP) emission spectrometry (SpectroCiros Vision, Spectro Analytical Instruments GmbH, Germany) and As(V) concentrations were analyzed as described earlier. The glass sample was finally removed and washed with acetone. They were then dried at 100 °C and weighed (Ramrakhiani et al. 2017).

Quality control/quality assurance

Quality assurance methods were applied in order to obtain accurate and meaningful data. The accuracy of arsenic analytical results in terms of the linear calibration curve and the SD between the replicates of results were assessed. The precision of arsenic analysis was tested on the instrument by analyzing four replicate samples with SD ranging between 0.5 to 1.4 for pH variation, 2.12–2.8 for dose deviation, 1.4–2.12 for temperature study, and 0.09–2.9 initial concentration variations. Hence, from the SD values, it is possible to examine the high repeatability of the analysis results. Care was also taken for use of contamination-free glasswares and other laboratory accessories required for NP synthesis, arsenic biosorption experiments, and analysis. All the glassware was washed with 50% (v/v) extran (phosphate-free), followed by 30% (v/v) nitric acid, and rinsed thoroughly with distilled and deionized water then oven-dried before use. The experimental workplace and heads were sterilized with HiCare Triclogel (HiMedia Laboratories Pvt., Ltd.).

Results and discussions

Synthesis of nanoparticles

Plant or plant part extracts serve as excellent reducing and stabilizing agents for bioreduction of metal NPs. In the present study, banana peel extracts served as the reducing and stabilizing agent needed for IONP formation. Banana peel extract has a high polyphenols and flavonoids content which allows efficient reduction of metal precursors to their corresponding NPs (Vu et al. 2018). The ratio of plant extract to 0.1 M FeCl$_3$ precursor was kept as 1:1. The formation of IONPs was monitored with color change. Upon addition of

the banana peel extracts to the precursor solution, the color of the reaction mixture immediately started changing within 2–5 min from yellow to black and indicated the generation of IONPs. Furthermore, the mixture was stirred at 500 rpm and 80 °C for 1 h for complete reduction of all the Fe^{3+} ions. Detailed characterizations of synthesized IONPs are presented in a later section.

Characterization of the IONPs: freshly prepared and As(V)-loaded

Figure 1A shows the XRD pattern of the synthesized IONPs. The characteristic diffraction peaks at $2\theta = 24.28°$, $33.27°$, $35.79°$, $40.99°$, $49.60°$, $54.16°$, $57.63°$, $62.55°$, $64.15°$, $71.91°$, and $75.62°$ corresponded to (012), (104), (110), (113), (024), (116), (112), (214), (300), (010), and (220) diffraction planes of hexagonal α-Fe_2O_3 (JCPDS card number 84-308; Popescu et al. 2011). The crystallite size as calculated using Scherrer's formula, $D = k\lambda/\beta\cos\theta$, where k is a constant with value of 0.9–1.0, λ is the X-ray wavelength, β is the full-width half maxima, and θ is the Bragg's angle which was estimated to be 38.28 nm (Mukherjee et al. 2016).

The elemental analysis of the IONPs before and after As(V) adsorption was carried out using XRF spectrometric analysis (Table 1a). The synthesized NPs revealed only the presence of Fe_2O_3 component, while after As(V) adsorption on IONPs, about 5.5 weight percentages of other elemental oxide compositions including arsenic, aluminum, phosphorus, sulfur, silica, potassium, calcium, etc. were observed. This is due to uptake of arsenic and other metals which were simultaneously present in the groundwater along with arsenic (Table 4).

FTIR spectra of α-Fe_2O_3 NPs (IONPs control adsorbent) and As(V)-loaded IONPs are shown in Fig. 1B. The IR spectrum of synthesized IONPs manifests prominent absorption bands located at 3384, 1624, and 665 cm^{-1}. The strong peak at 665 cm^{-1} indicates Fe–O–Fe
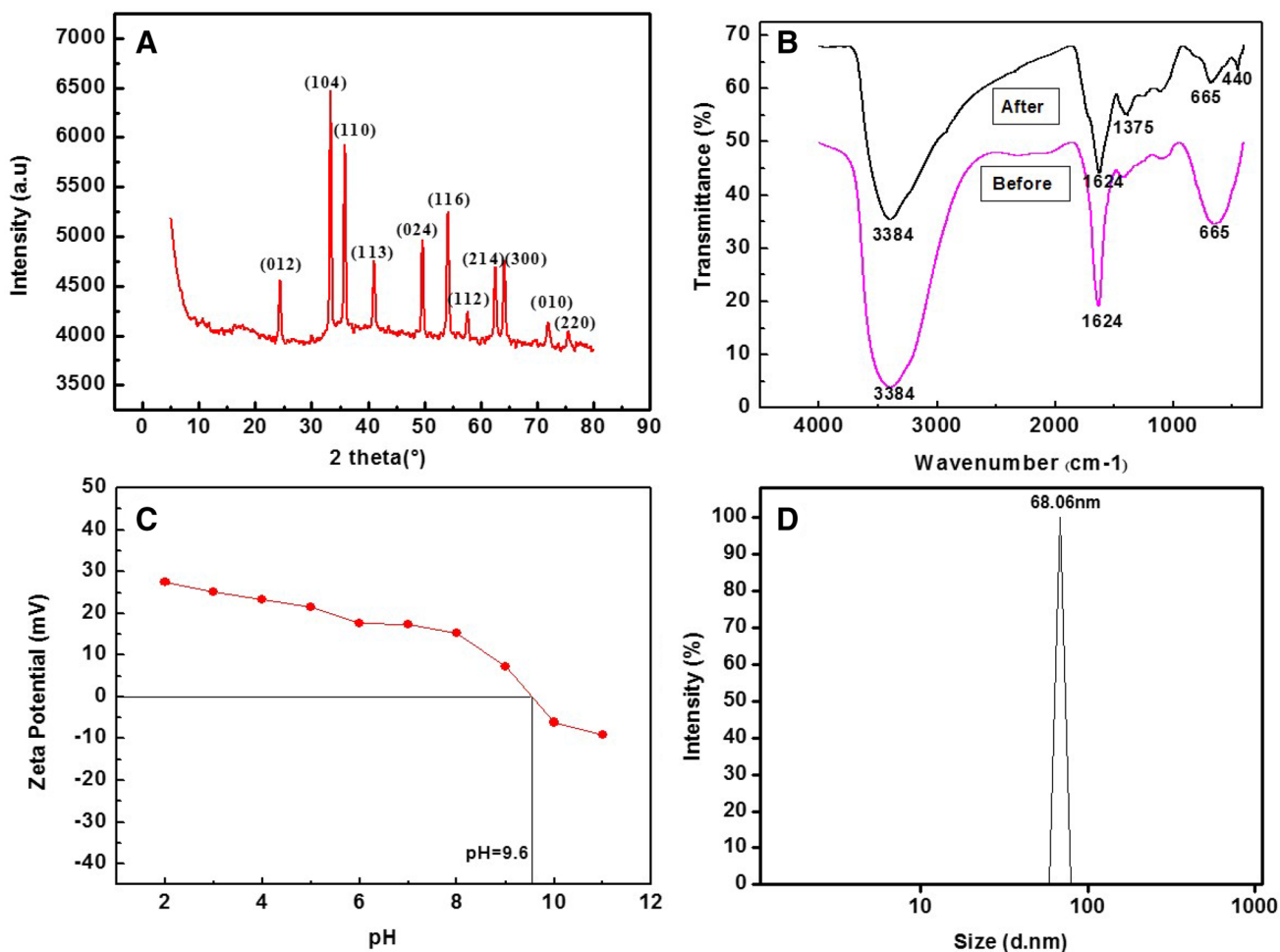

Fig. 1 Characterization of biologically synthesized IONPs using banana peel extracts: **A** XRD diffractogram of IONPs, **B** FTIR spectra of IONPs before and after As(V) adsorption, **C** zeta potential; **D** zetasizer

Table 1 Summary of XRF, FTIR, and XPS analysis of IONPs before and after As(V) adsorption

Sample number	Material name	Before adsorption (Wt%)	After adsorption (Wt%)
A. XRF analysis			
1	Fe_2O_3	100.00	94.511
2	As_2O_3	–	0.151
3	Al_2O_3	–	0.404
4	SiO_2	–	1.789
5	P_2O_5	–	0.390
6	SO_3	–	0.153
7	Cl	–	2.070
8	K_2O	–	0.282
9	CaO	–	0.250

FTIR peak	Synthesized IONPs as control adsorbent (wavelength cm^{-1})	IONPs After As(V) adsorption (wavelength cm^{-1})	Assignment
B. Frequency (cm^{-1}) and assignments of FTIR spectra			
1	–	440	As_2O_5
2	665	665	Fe–O–Fe stretching vibrations
3	–	1375	As_2O_5
4	1624	1624	C=O *str* in aldehyde and ketone
5	3384	3384	Hydrogen-bonded O–H (*str*)

Element	Binding energy (eV)		Atomic concentration (%)		Assignments
	Control IONPs	As-loaded IONPs	Control IONPs	As-loaded IONPs	
C. Results and assignments of high resolution of XPS spectral bands					
As 3*d*	–	45.23	–		As_2O_3 and As_3O_5 form of arsenic
Total As			–	4.24	
Fe2*p*	724.63	724.73	10.89	12.85	Fe 2*p* ½ satellite peak
	710.78	711.44	11.76	13.85	Fe_2O_3
Total Fe		22.65	26.7		
O 1*s*	531.03	531.30	17.74	19.75	Fe–O of Fe_2O_3 and As–O
Total O		17.74	19.75		
C 1*s*	287.59	288.30	7.65	9.29	C=O
	284.56	284.79	14.9	31.98	C–C
Total C		22.55	41.27		
N 1*s*	399.56	399.94	6.15	5.23	N, –NH$_2$, –NH–C–N, C=N,
	–	397.43	–	1.57	C–N, C=N,
Total N			6.15	6.8	

stretching vibrations of Fe_2O_3. The peaks of 3384 cm^{-1} and 1624 cm^{-1} are assigned to hydrogen-bonded O–H stretching (*str*) and C=O stretching vibration, respectively. The unreacted carboxyl group in aldehyde or ketone groups of secondary metabolites like phenols, flavonoids, etc. present in the banana peel extract may have given rise to C=O stretching vibrations at 1624 cm^{-1}.

After contact with As(V) solutions, the IONPs exhibited FTIR spectra with clear appearance of the bands at 440 cm^{-1} and 1375 cm^{-1}, which are specified as As_2O_5.

Comparative studies of the FTIR peaks of the adsorbent before and after adsorption are given in Table 1b. The significance of FTIR spectroscopy for recognition and characterization of synthesized IONPs from various processes was represented by Willis et al. (2005), Andrade et al. (2009), Mishra et al. (2013), and Mukherjee et al. (2016).

The specific surface area of the synthesized IONPs as obtained by multipoint BET method was found to be 11.47 m^2/g. The plot of zeta potential versus pH (Fig. 1C) showed the iso-electric point of IONPs at pH of 9.6. The

maximum zeta potential value of 27 mV existed at a pH of 2, after which the value gradually decreased with the increase in pH and reached negative at a pH of 10. The particle size measurement was based on the DLS method. The particle size was estimated by measuring their Brownian motion. The intensity-versus-diameter plot showed unimodal distribution with a d_{50} value of 68.1 nm (Fig. 1D).

The bright-field image (Fig. 2A) from TEM analysis revealed that the particles were cylindrical in shape. The lengths of the particles were around 60 nm which was comparable with the particle size estimated from zetasizer analysis and the crystallite size estimated from XRD. The polycrystalline structure of the synthesized adsorbent was evident from the ring patterns obtained from the selected-area diffraction pattern (SAED; Fig. 2B). The $d_{spacing}$ values from the SAED pattern matched those of the XRD data, confirming the presence of (110), (113), (116), (112), and (214) planes (Ibrahim 2015).

FESEM-EDX analysis

FESEM micrographs of the control and the arsenic-loaded IONPs are presented in Fig. 3A and B, respectively. The As-loaded IONP micrograph indicated morphological changes as agglomeration when compared to that of control IONP. The EDX spectra of As-loaded adsorbent revealed an arsenic peak, while no such peak could be found on the control adsorbent surface. This confirms the morphological changes due to the presence of arsenic on the IONP (Fig. 3C, D).

XPS facilitates chemical-state surface analysis, quantitative elemental composition, and determination of metal oxidation states in the IONP samples. The wide-scan XPS spectrum of control IONP samples shows the photoelectron lines at binding energies at 709.24, 529.77, 399.17, and 285.83 eV are attributed to Fe2p, O1s, N1s, and C1s, respectively (Fig. 4A). The XPS spectrum of arsenic-loaded IONPs indicated an additional peak at a binding energy of 45.23 eV, which is assigned for As3d (Fig. 4B). The high-resolution XPS spectrum of As3d after As(V) adsorption revealed a remarkable increase in peak size at a binding energy of 45.23 eV and % atomic concentrations (%AC) of 4.24, that signified the successful As(V) binding to IONPs (Fig. 4C and Table 1C). The deconvolution of Fe2p spectra of both control and As(V)-loaded IONPs created two peaks. The binding energy and %AC values of Fe_2O_3 were 710.78 eV and 11.76% in the control IONPs, and 711.44 eV and 13.85% for As(V)-loaded IONP samples. The separated small peak at 724.63 eV (in the control) and 724.73 eV (in As-loaded IONPs) were denoted as a satellite peak in pure Fe_2O_3 state (Fig. 4D and E). In XPS data analysis, since oxygen, carbon, and nitrogen can change the reactivity of surfaces, their spectra are significant for adsorption studies. High-resolution O1s spectra for both the control and As-loaded IONP samples produced a single peak at 531.03 and 530.30 eV, respectively, that can be attributed to the oxygen of the IONPs (Gallegos-Garcia et al. 2012). The shift in binding energy as well as increase in O1s peak area, i.e. increased in %AC from 17.74 to 19.75 were observed in the As(V)-loaded sample, which indicated the adsorption of arsenic onto the surface of the NPs (Fig. 4F and G and Table 1C). The deconvolution of C1s spectra of the control and As-loaded IONPs created two peaks with binding energies of 287.59 and 284.56 eV, and 288.30 and 284.79 eV, respectively; this represented the functional groups of C–H and/or C–C, C–O, C=O, and O–C=O (Fig. 4H and I). After arsenic adsorption on the surface of IONPs, a shift in
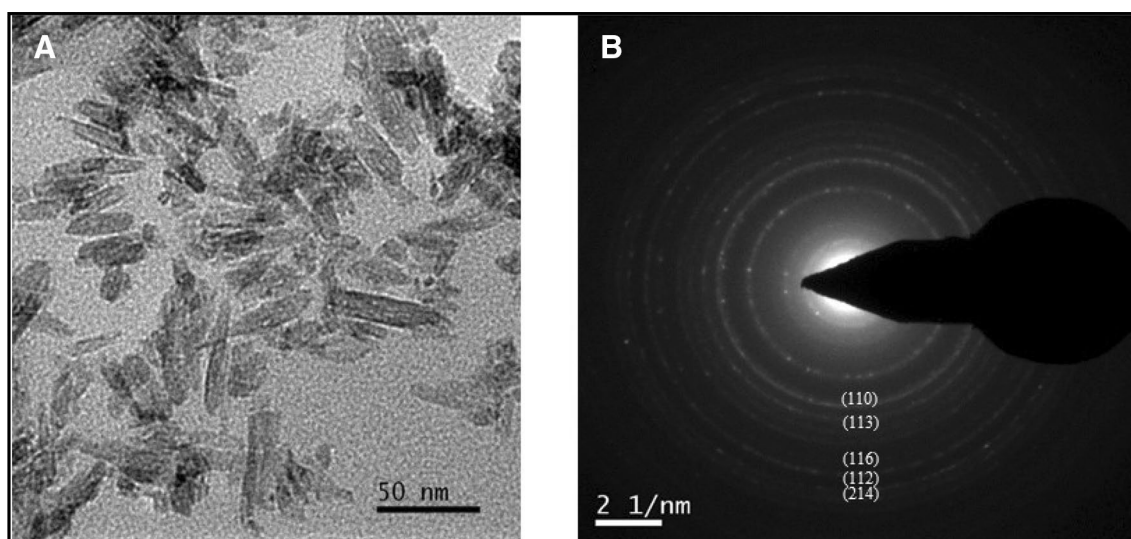

Fig. 2 TEM analysis **a** bright-field images of α-Fe_2O_3, **b** SAED pattern of α-Fe_2O_3
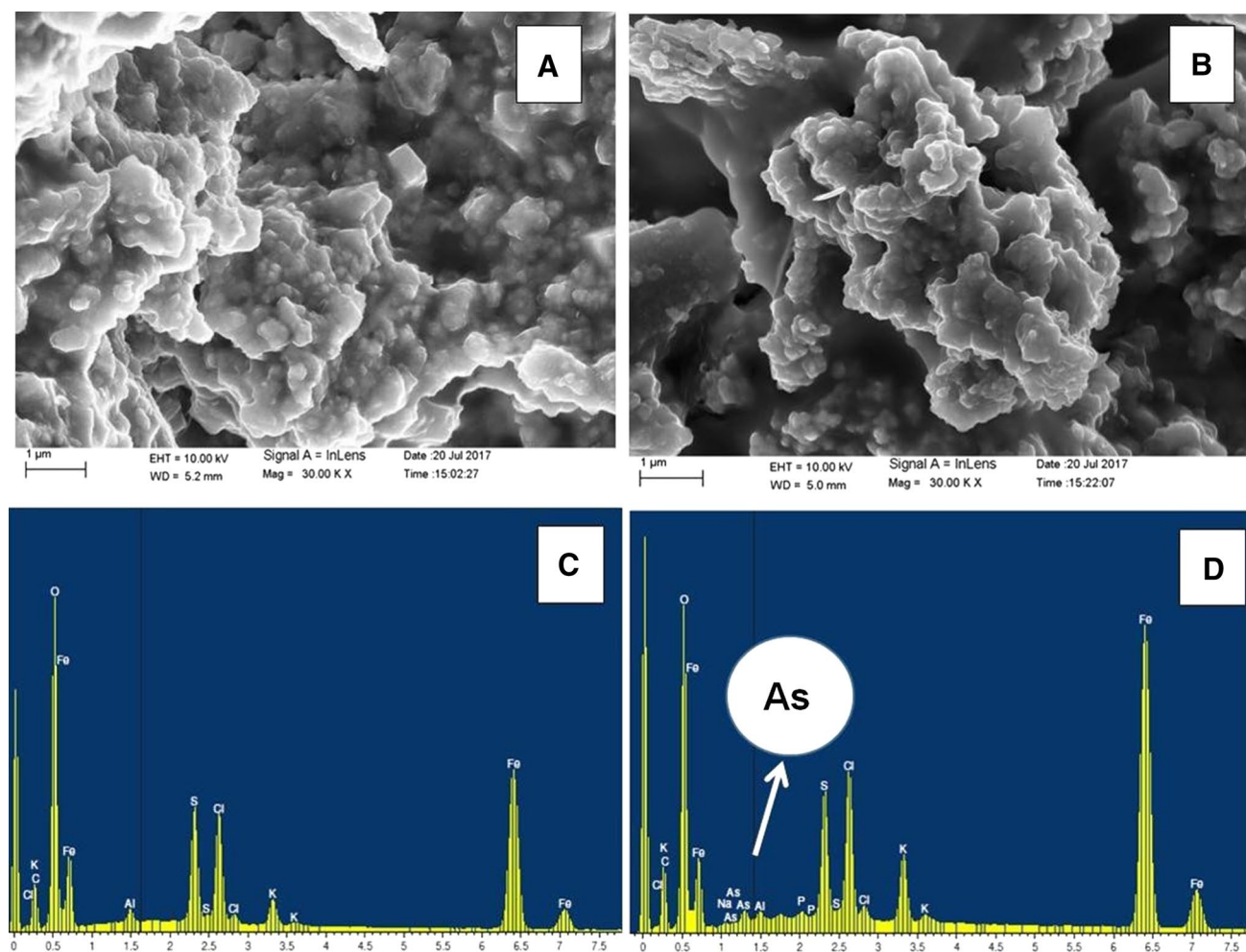
Fig. 3 FESEM-EDX analysis. **A** FESEM micrographs of iron oxide nanoparticles (control IONPs), **B** FESEM micrographs of arsenic-loaded IONPs, **C** EDX spectra of control IONPs, **D** EDX spectra of arsenic-loaded IONPs

binding energies and an increase in %AC, indicated oxidation of the carbon surface due to arsenic adsorption/deposition (Table 2; Chowdhury et al. 2011). Deconvolution of the N1s spectra of the control and arsenic-loaded IONPs generated one and two peaks with binding energies of 399.56 eV, and 399.94 and 397.43 eV, respectively (Fig. 4J, K). The appearance of an additional peak on the arsenic-loaded IONP XPS spectra and an increase in the %AC denoted involvement of nitrides and organic components in arsenic binding. The XPS analysis demonstrated the surface binding of arsenic on the green-synthesized IONPs.

Arsenic(V) adsorption studies

Effect of pH of water matrix

Experiments concerning the effect of pH on As(V) adsorption by the synthesized IONPs were carried out within a pH range from 2 to 10, while the adsorbent dosage,

reaction temperature, and initial As(V) concentration remained constant at 1 g/L, 20 °C, and 1 mg/L, respectively. Adsorption was found to be favorable in acidic pH and was constant till the pH of 6. However, at alkaline pH, there was a significant drop in As(V) adsorption. The finding can be explained with the help of zeta potential data of the adsorbent and the dissociation of As(V), as shown in Fig. 1C. The adsorbent showed a steady net positive charge till pH 8.0, after which it starts shifting towards the negative side. The point of zero charge for the adsorbent was found to be at a pH of 9.6. According to the Eh–pH diagram, As(V) exists as negatively charged $H_2AsO_4^-$ (at pH between 2 and 6.9) and $HAsO_4^{2-}$ (at pH above 6.9; Smedley and Kinniburgh 2002). It can be inferred that the net positive charge on the synthesized IONPs facilitated high adsorption till pH 8.0. Due to the electrostatic interaction between the positively charged adsorbent and negatively charged arsenate ions, the chemisorption process gets enhanced at acidic pH (Martínez-Cabanas et al.
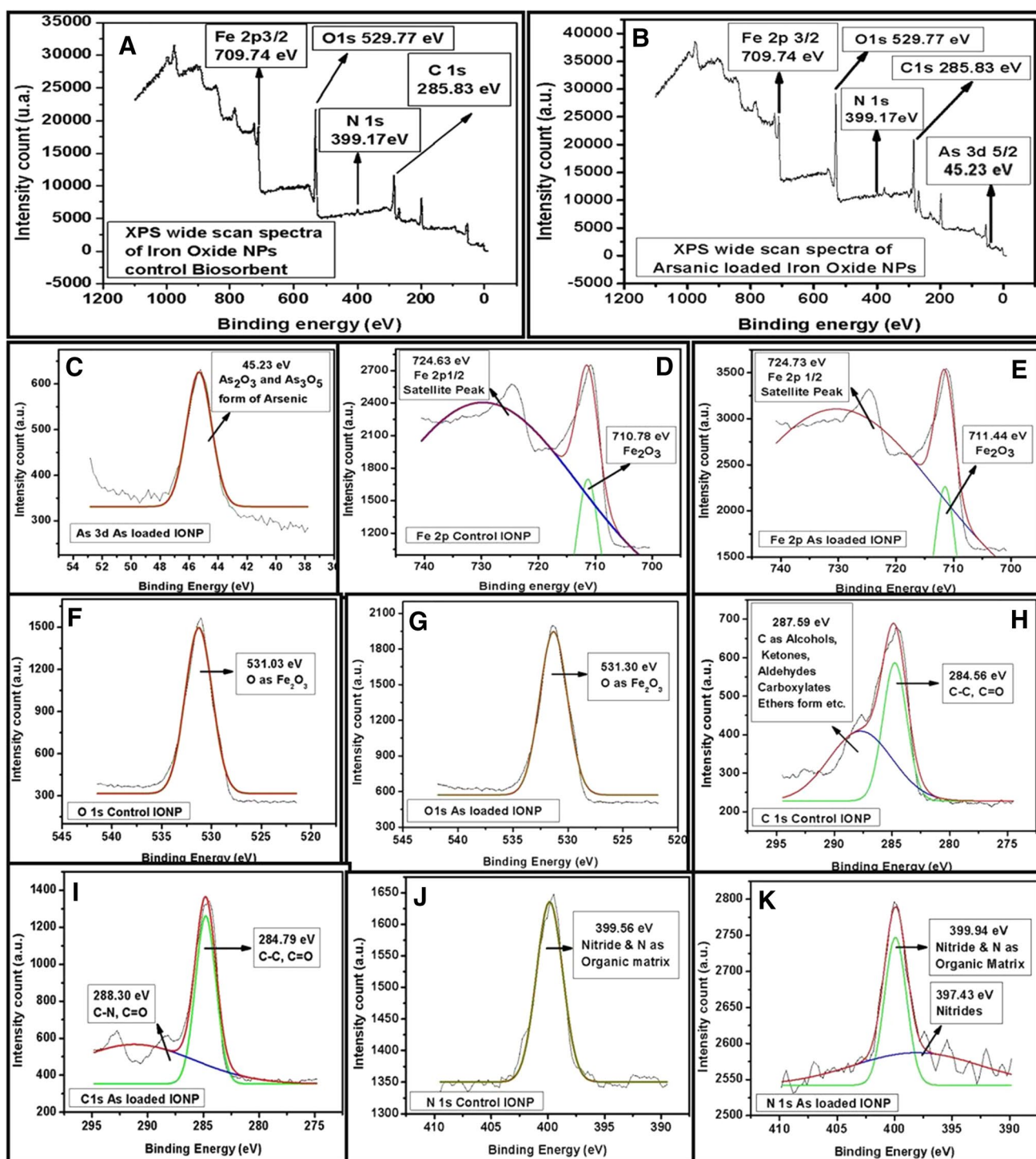
Fig. 4 XPS spectra of IONP adsorbent. **A** Wide-scan spectra of control adsorbent; **B** wide-scan spectra of arsenic-loaded adsorbent; **C** As 3*d*; **D** Fe 2*p* control IONP; **E** Fe 2*p* arsenic-loaded IONP; **F** O1*s* control adsorbent; **G** O1*s* arsenic-loaded adsorbent; **H** C1*s* control IONP; **I** C1*s* arsenic-loaded adsorbent; **J** N1*s* control IONP; **K** N1*s* arsenic-loaded adsorbent

2016). The significant drop in adsorption at higher pH may be because the adsorbent exhibits negative charge at alkaline pH and there may be electrostatic repulsion between the adsorbent and the negatively charged As(V)

ions. The optimized value of pH was selected at pH 6.0 for easy reproducibility in practical pH conditions of arsenic-contaminated groundwater. The influence of pH on As(V) removal efficiency is depicted in Fig. 5A.

Table 2 Langmuir isotherm, Freundlich isotherm, and kinetics parameters for As(V) adsorption onto biologically synthesized iron oxide nanoparticles

Temp. (°C)	Langmuir isotherm					Freundlich isotherm			
	Q_{max} (mg g^{-1})	b (L mg^{-1})	R^2	RMSE	k_f	n	R^2	RMSE	
Isotherm study									
20	1.774	5.139	0.9787	0.049	3.735	1.214	0.9922	0.03321	
30	2.325	4.826	0.9979	0.01796	4.309	1.306	0.9932	0.03257	
40	2.715	4.335	0.9995	0.00920	5.137	1.251	0.9982	0.01679	
As(V) concentration (mg L^{-1})	Pseudo first-order kinetic model				Pseudo second-order kinetic model				
	K_1	Q_e calc (mg/g)	R^2		K_2	Q_e calc (mg/g)	R^2		
Kinetics study									
0.1	0.68	0.013	0.8486		7.68	0.96	0.999		
1	0.75	0.1289	0.7882		7.9	0.47	0.998		
2	1.43	0.252	0.8573		82.36	0.050	0.998		

RMSE root mean squared error

Effect of adsorbent dose

For effective As(V) sorption, adsorbent dose is a significant factor that determines the sorbent–sorbate equilibrium of the system. It also establishes the number of binding sites available for adsorption. The results demonstrated significant increase in the removal efficiency from 81 to 93% at equilibrium when the adsorbent dose was increased from 0.5 to 2.0 g/L. However, on further increase in the adsorbent dose, there was no considerable enhancement in removal efficiency, but a significant decrease in the adsorption capacity; hence, an adsorbent dose of 2 g/L was chosen as the optimized dose. The influence of adsorbent dose on As(V) removal efficiency is depicted in Fig. 5B.

Effect of temperature and initial concentration

The influence of temperature on As(V) removal efficiency was evaluated varying the temperature from 20 to 40 °C (Fig. 5C). Maximum removal efficiency of 95.5% was obtained at a temperature of 40 °C. Maximum removal efficiency of 96% was observed at an initial concentration of 0.5 mg/L. The influence of initial concentration on As(V) removal efficiency is depicted in Fig. 5D. The adsorption capacity increased with increasing As(V) concentration because more As(V) species were available for adsorption. The removal efficiency dipped from 95.5 to 93.5% at equilibrium when the initial concentration was increased from 0.5 to 2.0 mg/L.

Adsorption isotherm

The adsorption process was carried out at three different temperatures viz., 20, 30, and 40 °C. The initial As(V)

concentration was varied from 0.1 to 2 mg/L. The adsorption data were fitted to Langmuir and Freundlich isotherm models (Eqs. 8 and 9, respectively), as depicted in Fig. 5E. Langmuir and Freundlich isotherms have universally been used to describe arsenic adsorption. The value of model constants, R^2, and RMSE are given in Table 2. The high values of R^2 and low values of RSME indicate that the adsorption fitted well with both the Langmuir and Freundlich isotherm model (An et al. 2016; Yu et al. 2017). The values of separation factor $r(1/[1 + b*C_e])$, was always less than 1, indicating favorable adsorption.

$$Q_e = \frac{Q_{max} * b * (C_e)}{1 + b + C_e} \tag{9}$$

$$Q_e = k_f * \sqrt[n]{C_e} \tag{10}$$

where Q_e (mg/g) is the adsorption capacity at equilibrium, C_e (mg/L) is the solute concentration at equilibrium, Q_{max} (mg/g) is the maximum adsorption capacity, b (L/mg) is the Langmuir constant representing the affinity between the solute and the adsorbent, k_f is the Freundlich constant, and n is the adsorption intensity ($1 < n < 10$). The Langmuir isotherm suggested monolayer adsorption, while the Freundlich isotherm assumed multilayer adsorption. It was found that both the Langmuir and Freundlich isotherms were able to describe the adsorption process (Table 2). This indicated both multilayer and monolayered adsorption taking place.

Thermodynamics study

The values of three thermodynamic constants, $\Delta G°$ as Gibb's free energy (in J mol^{-1}), $\Delta H°$ as the enthalpy change (in
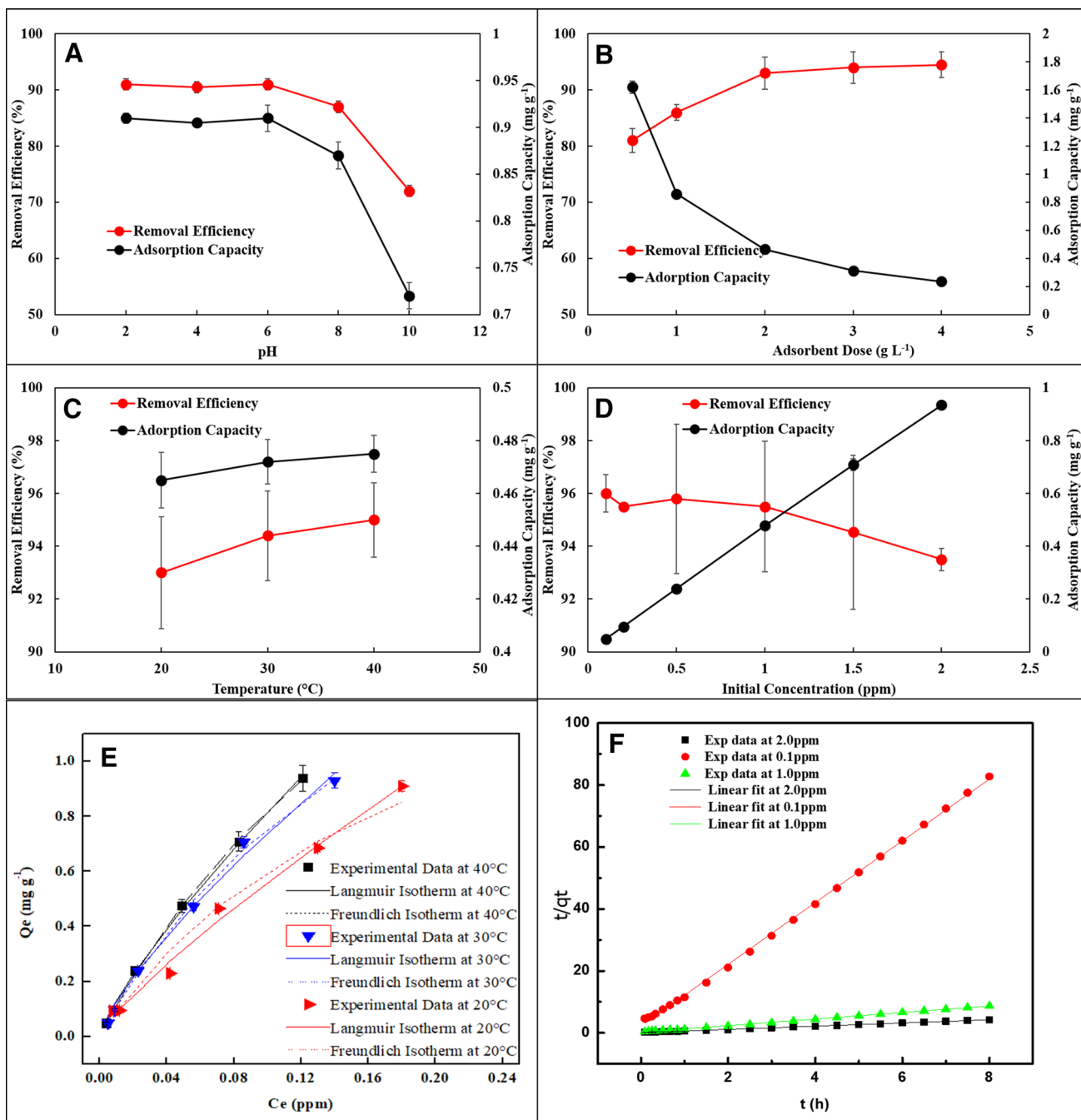
Fig. 5 Adsorption process optimization for As(V) removal by biologically synthesized iron oxide nanoparticles (IONPs) **A** influence of pH; **B** influence of adsorbent dose; **C** temperature °C; **D** influence of initial concentration of As(V); **E** adsorption isotherms for the As(V) Langmuir and Freundlich isotherms; **F** Pseudo second-order kinetic study

$J \, mol^{-1}$), and $\Delta S°$ as the entropy change (in $J \, mol^{-1} \, K^{-1}$) were calculated from Eqs. (10) and (11).

$$\Delta G° = -RT \ln b \tag{11}$$

$$\Delta G° = \Delta H° - T\Delta S° \tag{12}$$

where R is the universal gas constant ($R = 8.314 \, J \, mol^{-1} \, K^{-1}$), b is the equilibrium constant as obtained from isotherm fitting, and T is the temperature in Kelvin. $\Delta G°$ for three different reaction temperatures viz. 20, 30, and 40 °C were found to be $-20,814.7 \, J \, mol^{-1}$, $-21,366.8 \, J \, mol^{-1}$ and $-21,792.8 \, J \, mol^{-1}$, respectively (Eq. 9). The values of $\Delta H°$ and $\Delta S°$ of the adsorption process obtained from the intercept and the slope of Eq. (10) were found to be $-6507.2 \, J \, mol^{-1}$ and $48.9 \, J \, mol^{-1} \, K^{-1}$, respectively. The

values of $\Delta G°$ were negative and they decreased with the increase in temperature. These values suggested a spontaneous nature of adsorption and supported the fact that better adsorption takes place at higher temperature. That can be confirmed by the higher values of Q_{max} at higher temperatures. The negative value of $\Delta H°$ indicates that the system has released heat and, thus, it can be concluded that the adsorption process was exothermic. The positive values of $\Delta S°$ indicate that chemisorption has taken place and there has been variation in surface structure and breakage of bonds differing in strength (Jing et al. 2010).

Kinetics study

To study the kinetics of As(V) adsorption by the synthesized IONPs, the initial concentration of As(V) solutions was varied (0.1, 1.0, and 2.0 mg/L) and adsorbent dosage of 2 g/L, solution pH at 6 and reaction temperature 40 °C were taken. Samples were collected at regular intervals and analyzed for As(V) concentration. The adsorption rate was described by employing Lagrange's first-order kinetics model and pseudo-second-order kinetics model in the study. The linear integral forms of the kinetic models are described below (An et al. 2016).

$$\ln(q_e - q_t) = \ln q_e - k_1 t \qquad (13)$$

$$\frac{t}{q_t} = \frac{1}{k_2 q_e^2} + \frac{1}{q_e} * t \qquad (14)$$

where q_t (mg g^{-1}) is the amount of As(V) adsorbed at time t (h), q_e is the metal uptake at equilibrium, k_1 (h^{-1}) is the adsorption rate constant for the first-order kinetics, k_2 (g mg^{-1} h^{-1}). For the first-order kinetics, t was plotted against $\ln(q_e - q_t)$. Straight lines were fitted by regression and the value of k_1 was calculated from the slope of the equation of the formed straight lines. For the pseudo-second-order kinetic model, t was plotted against t/q_t and the value of k_2 was obtained from the intercept of the straight line formed from the plot. The values of k_1, k_2, q_e, and R^2 are given in Table 2. The experimental results suggested that the equilibrium was reached within 2 h of the study. A better linear fit was observed for the pseudo-second-order kinetic model (Fig. 5f) compared to the pseudo-first-order kinetic model, indicating chemisorption to have taken place.

Mechanism for arsenic adsorption

The high negative values of enthalpy indicated an exothermic process. Breaking of bonds and alteration of the adsorbent surface were indicated by a negative entropy value. The change of surface of the adsorbent was vivid from FESEM images of As-loaded IONPs. Appearance of 2 peaks at 440 cm^{-1} and 1375 cm^{-1} in the FTIR spectrum of As-loaded IONPs are assigned to As$_2$O$_{5.}$ This indicates that As(V) adsorption has altered the surface functional groups of IONPs. The adsorption of arsenic on the surface of the adsorbent occurs in a few stages. Initially, a hydrolysis reaction occurs between the surface of the IONPs and the aqueous solution. The hydroxyl ions of the water get attached to the Fe–O–Fe bonds and forms oxyhydroxides. A nucleophilic reaction occurs between the arsenate ions and hydroxyl ions. As a result, the arsenate ions get attached to the Fe–O–Fe bonds (Mercado-Borrayo et al. 2014). This may result in the weakening of Fe–O–Fe stretching vibrations at 665 cm^{-1}. Elemental analysis by EDX and XRF of both freshly prepared and As-loaded adsorbent indicated presence of arsenic in the adsorbent. Further appearance of a peak at 45.23 eV in the XPS spectrum of the As-loaded IONPs and atomic concentration of 4.24% indicates binding of As(V) on to the IONPs. Adsorption of arsenic at acidic pH indicated electrostatic repulsion to have existed between the adsorbate and the adsorbent. The negatively charged As(V) species are easily attracted to the positively charged IONPs, having point of zero charge at 9.6, at a pH of 6. These observations indicate chemisorption to have taken place on the surface of the IONPs.

ANN modelling

The network with the maximum R^2 value and minimum MSE value was chosen as the optimal network. The number of neurons in the hidden layer was varied from 1 to 30 and its dependence on the corresponding MSE and R^2 values for the LM algorithm was studied. The variation in MSE values and R^2 values with the change in number of neurons in the hidden layer is shown in Table 3. The network provided a maximum R^2 value of 0.9971 and the corresponding MSE value was 0.0000601 when the number of neurons in the hidden layer was 11. Since the correlation coefficient is very high, the developed ANN model can be called reliable. The optimized architecture can be defined as ANN (4-11-1) containing 1 input layer with 4 neurons, 1 hidden layer with 11 neurons, and 1 output layer with 1 neuron. The best validation performance was obtained at epoch 5 and the training was stopped. Figure 6A depicts the regression plot of the normalized experimental data versus normalized model-predicted data of all the data. The graph clearly shows that there was an excellent agreement between the experimental data and the data predicted by the model. The weights and biases of the final optimized architecture are given in Table 3. The

Table 3 Comparison of MSE and R^2 values at different numbers of neurons present in the hidden layer for the artificial neural network model developed by the Levenberg–Marquardt algorithm

Neuron number	MSE	R^2	Neuron number	MSE	R^2	Neuron number	MSE	R^2
Neuron study								
1	0.00345	0.660969	11	0.000060	0.994208	21	0.000697	0.9409
2	0.000689	0.935089	12	0.00148	0.876096	22	0.00161	0.851929
3	0.000421	0.958441	13	0.00301	0.734449	23	0.00495	0.6561
4	0.000533	0.948676	14	0.000635	0.938961	24	0.000399	0.968256
5	0.00106	0.896809	15	0.000624	0.938961	25	0.00263	0.906304
6	0.000171	0.984064	16	0.00116	0.906304	26	0.00506	0.6561
7	0.00127	0.885481	17	0.00152	0.863041	27	0.00522	0.591361
8	0.00107	0.904401	18	0.00017	0.982081	28	0.00993	0.434281
9	0.000525	0.970225	19	0.00105	0.900601	29	0.0108	0.294849
10	0.000777	0.925444	20	0.00152	0.872356	30	0.0158	0.2401
IW				LW		b_1		b_2
The weight and bias values of hidden and output layers for the optimally trained artificial neural network								
−1.76202	0.320514	1.209648	1.161309	0.107756	2.839267	0.59106		
−2.29165	1.457515	1.796262	− 1.0547	− 0.009	0.921873			
−2.2694	0.795707	− 0.28523	− 0.37501	0.790319	1.294659			
−0.70997	0.577592	2.949336	0.311203	0.183739	1.286193			
−0.98984	1.558044	− 1.41094	− 1.95545	− 0.12404	0.69139			
−0.7781	1.318681	1.045169	− 1.70617	− 0.03578	0.26981			
1.152221	0.307441	− 0.64567	0.147827	0.645005	0.876139			
1.385922	− 1.9285	− 1.95727	0.415255	− 0.09971	− 0.13557			
−1.55794	− 0.11357	2.025524	− 0.38059	0.348932	− 1.99126			
2.390519	− 1.44535	1.064396	− 1.26638	0.070636	2.299785			
−0.95282	− 1.91355	1.883549	0.217526	− 0.36198	− 2.37132			

MSE mean squared error; *IW* initial weight of the hidden layer; *LW* weight of the output layer
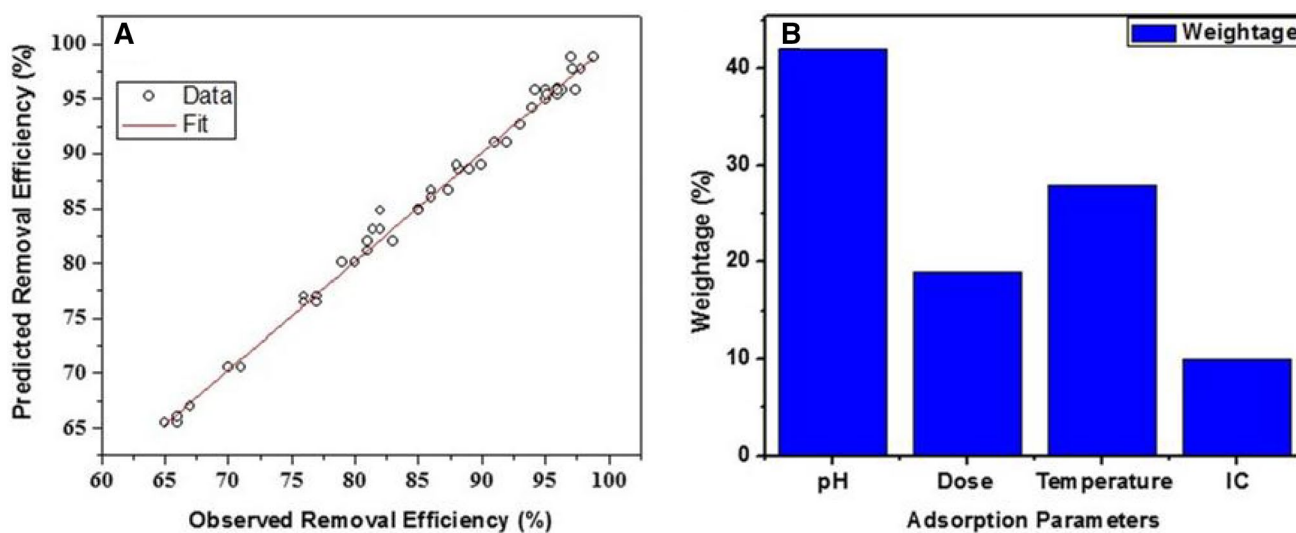

Fig. 6 a Scatter plot between normalized model-predicted removal and normalized experimental removal for all data; for the adsorption of As(V) onto α-Fe₂O₃ nanoparticles; **b** dependence of removal efficiency on the adsorption parameters

inputs and the outputs of the model can be correlated by the fitness function of the model which may be defined as

$$\text{ANN output} = \text{Purelin} (LW * \text{tansig} (IW*[x(1);x(2);x(3);x(4)] + b_1) + b_2) \tag{15}$$

where IW is the initial weight of the hidden layer, b_1 is the initial bias of the hidden layer, LW is the weight of the output layer, b_2 is the bias of the output layer, and $x(1)$, $x(2)$, $x(3)$, and $x(4)$ are the inputs. The experimental outputs and the ANN model outputs are given in Table S1.

The relative importance of each adsorption parameter in the adsorption process was estimated by conducting a sensitivity analysis. Connection weight partitioning methodology was used to carry out the sensitivity analysis (Debnath et al. 2016a, b). The relative effect of each adsorption parameter was estimated using the following equation:

$$V = \frac{X}{\sum_{j=1}^{m} X} * 100 \tag{16}$$

$$X = \sum_{j=1}^{h} \left[\left(\frac{|IW_{ij}|}{\sum_{k=1}^{m} |IW_{kj}|} \right) |LW_j| \right] \tag{17}$$

where V is relative effect of the adsorption parameter (i) in percentage, m is the number of adsorption parameters or the number of neurons in the input layer, and h is the number of neurons in the hidden layer. The relative effects of each of the adsorption parameters or the input variables were calculated using Eqs. 15 and 16 and are shown in Fig. 6B. It was evident from the result that pH was the most influential factor in the adsorption process. Temperature had more effect as compared to dose, while the initial concentration

had the least effect on adsorption. This coincides with the findings of our experiments. pH was indeed the driving factor behind the adsorption process because electrostatic attraction between the negatively charged As(V) species and positively charged IONPs played a significant part. Also, from the thermodynamics study, we concluded that the process is exothermic and chemisorption had taken place. Also, better removal was obtained at higher temperatures, which is reflected in the sensitivity analysis of the model. Effect of dose and initial concentration were less influential because adsorption did not significantly vary with variation in these two parameters.

As(V) removal from a contaminated groundwater system

The collected arsenic-contaminated groundwater was treated with the synthesized IONPs as adsorbent at optimized conditions. Both the contaminated groundwater and the treated water were analyzed for presence of As(V) and other ions. The concentrations of the various ions present in the water sample before and after adsorption are given in Table 4. As(V) was successfully reduced below the permissible limit of 0.01 mg/L along with considerable reduction of Ca, Na, Mg, K, F, and Cl ions present. More than 98% removal was observed for the ions, while 94.97 and 61.53% of Cl and F were removed, respectively. Thus, it can be concluded that the synthesized adsorbent was not only efficient in removal of As(V) in synthetic medium but equally capable of removing As(V) along with other impurities from contaminated groundwater.

Table 4 Results of ground water treatment and results of leaching test of prepared glass

Impurities in raw groundwater	Ca (mg L^{-1})	Mg (mg L^{-1})	Na (mg L^{-1})	K (mg L^{-1})	F (mg L^{-1})	Cl (mg L^{-1})	As(V) (mg L^{-1})
Ground water study							
Untreated ground water	102.29	29.63	20.33	1.91	0.13	21.3	0.6
Treated ground water	1.81	0.03	ND	ND	0.05	1.07	0.012

| No. of days	Fe (µgL^{-1})	P (µgL^{-1})	Si (µgL^{-1})	As (µgL^{-1})	Method
Leaching test results					
7	ND	0.4	0.07	BDL	ICP
14	0.06	0.84	ND	BDL	ICP
21	ND	1.13	ND	BDL	ICP
28	ND	1.22	ND	BDL	ICP

BDL Below detection level; *ND* not detected

Table 5 Comparison of maximum adsorption capacity of synthesized iron oxide nanoparticles with various adsorbents reported in literatures for removal of arsenic from aqueous solution

Adsorbent	Adsorption capacity (mg g^{-1})	Initial concentration (mg L^{-1})	References
Zero-valent iron	1.2	1	Kanel and Choi (2017)
Industrial byproducts	0.96	1	Kanel and Choi (2017)
Magnetite Fe_3O_4	0.147	0.3–8	Martínez-Cabanas et al. (2016)
3D Fe_3O_4/graphene	0.385	0.1–1	Liu et al. (2015)
Leonardite loaded with ferric ions	0.322	0.1–0.4	Solé-Sardans et al. (2016)
Charred dolomite	2.157	0.05-2.0	Salameh et al. (2015)
Coal-based mesoporous activated carbon	1.76	0.1–0.5	Li et al. (2014)
Acidified laterite	0.9236	0.1	Glocheux et al. (2013)
Iron oxide-coated sand and limestone	0.075	0.2–20	Devi et al. (2014)
Green-synthesized α-Fe_2O_3 nanoparticles	2.715	0.1–2.0	This study

Comparison of arsenic removal using other adsorbents

A lot of research has been focused in the recent years to develop an effective adsorbent for As(V) removal from groundwater or a medium with low arsenic concentrations. The various kinds of adsorbents that have been used are IONPs, iron oxide, reduced graphene oxide composites, iron oxide-coated materials, zero-valent iron, laterite, dolomite, activated carbon, industrial byproducts, and many more. The list of adsorbents and their As(V) adsorption capacities are mentioned in Table 5 (Glocheux et al. 2013; Devi et al. 2014; Salameh et al. 2015; Liu et al. 2015; Cheng et al. 2016; Solé-Sardans et al. 2016; Martínez-Cabanas et al. 2016; Kanel and Choi 2017). The maximum adsorption capacity of banana peel-synthesized,

hexagonal α-Fe_2O_3 was found to be 2.715 mg g^{-1} at a pH and temperature of 6 and 40 °C respectively, which was much higher than most of the adsorption capacities of other adsorbents at low initial As(V) concentrations. This can be attributed to various factors. The isoelectric point for the synthesized IONPs was at a pH of 9.6 which indicates that the adsorbent exhibits a high positive charge of around 20 mV at near neutral pH (6–7). This facilitated better adsorption. Also, the presence of Fe–O–Fe stretching vibrations as observed in the FTIR spectra at 665 cm^{-1} play significant role in chemisorption. Also, the much smaller particle size (~ 60 nm) provided more surface area for adsorption as compared to other adsorbents (Glocheux et al. 2013; Salameh et al. 2015). The surface area of our synthesized IONPs was 11.47 m^2/g which was
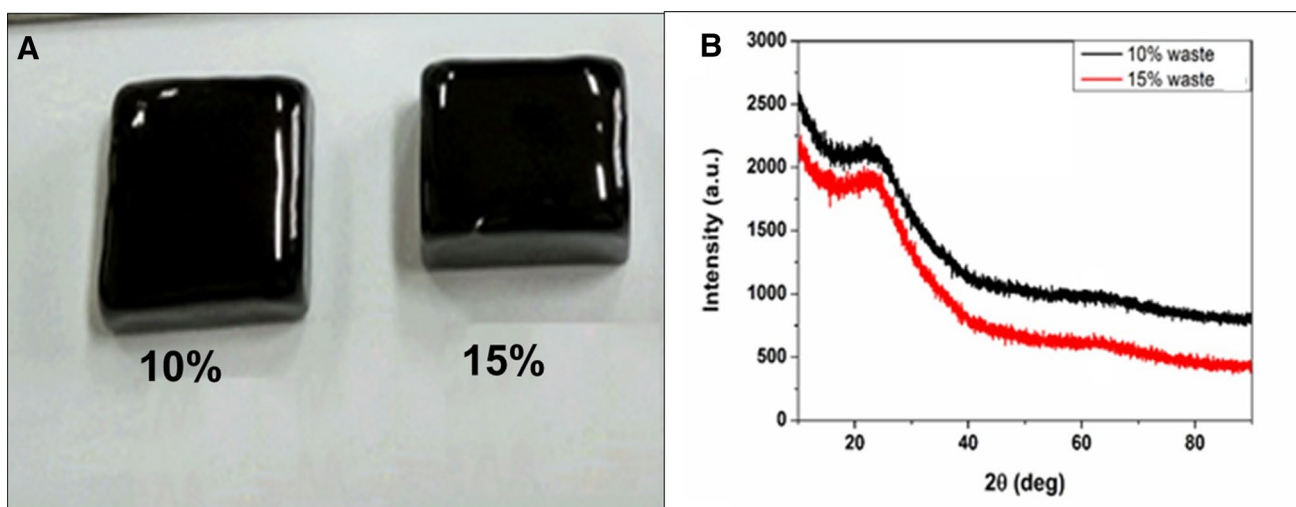
Fig. 7 Inertization of 10 and 15% arsenic-loaded IONPs in phosphate glass matrix. **a** Photograph of prepared glass; **b** XRD diffractogram of prepared glass

larger than that of zero valent iron (0.9 m^2/g) and industrial byproducts (5 m^2/g) (Kanel and Choi 2017).

Safe disposal of exhaust adsorbent: incorporation in glass matrix

Encapsulations of arsenic-loaded, exhausted spent adsorbent into phosphate glass matrix were considered as a safe mode for discard to the environment. About 10 and 15% of the spent adsorbent was incorporated in the formulation of phosphate glass composition (Fig. 7a). XRD analysis was conducted on the prepared glasses to determine the crystalline and noncrystalline phases. The XRD spectra of both the prepared glasses having 10 and 15% of spent adsorbent incorporated revealed noncrystalline phases, thus confirming the formation of glass (Fig. 7b). Although, only 20% of the spent adsorbent has been incorporated for glass formation in this study, attempts to incorporate more of the spent adsorbent in the glass matrix are under progress.

Results of dissolution experiments conducted with deionized water heated at 75 °C for 6 h per day for 28 days showed no weight loss of the glass and the glass had the same appearance as that of the polished glass. The dissolution test results given in Table 4 indicate no leaching of the hazardous metal ions. The leaching test values indicated no leaching of As(V) or Fe which were incorporated into the glass. Thus, the glass can be recommended for the incorporation of spent iron-based adsorbents for entrapment of hazardous metal ions for its disposal in an environmentally safe manner.

Conclusion

Banana peels as agricultural waste material was effectively utilized for the quick and consistent synthesis of IONPs. XRD, FTIR, TEM, and FESEM analysis confirmed formation of cylindrically shaped α-Fe$_2$O$_3$ with an average particle size of around 60 nm. The biosynthesized IONPs were successfully applied as suitable adsorbent for arsenic(V) removal from contaminated groundwater. Comparisons of arsenic removal efficiency using various adsorbent were conducted. The maximum adsorption capacity of banana peel-synthesized IONPS was found to be 2.715 mg/g at pH 6.0 and temperature 40 °C, which was much higher than most of the adsorption capacities of other adsorbents at low initial As(V) concentrations. ANN-based optimization study revealed that pH was the most influential factor in the adsorption process. The sludge management strategy was proposed in the present study. The arsenic-loaded hazardous IONPs up to 20% were inertized as phosphate glass formations, which can be considered as an environmentally

safe and productive option. The prepared phosphate glass containing 15% spent IONPs exhibited no leaching of arsenic and iron ions up to 28 days of dissolution testing using deionized water with a thermal cycle at 75 °C for 8 h/day. Hence, this study proves to be an efficient and complete process for As(V) remediation from contaminated water with a striking strategy for toxic sludge management.

References

Ali I (2012) New generation adsorbents for water treatment. Chem Rev 112:5073–5091. https://doi.org/10.1021/cr300133d

An C, Yang S, Huang G et al (2016) Removal of sulfonated humic acid from aqueous phase by modified coal fly ash waste: equilibrium and kinetic adsorption studies. Fuel 165:264–271. https://doi.org/10.1016/J.FUEL.2015.10.069

Andrade AL, Souza DM, Pereira MC, Fabris JD, Domingues RZ (2009) Synthesis andcharacterization of magnetic nanoparticles coated with silica through a sol-gel approach. Cerâmica 55:420–424. https://doi.org/10.1590/S0366-69132009000400013

Brunson LR, Sabatini DA (2009) An evaluation of fish bone char as an appropriate arsenic and fluoride removal technology for emerging regions. Environ Eng Sci 26:1777–1784. https://doi.org/10.1089/ees.2009.0222

Bundschuh J, Maity JP (2015) Geothermal arsenic: occurrence, mobility and environmental implications. Renew Sustain Energy Rev 42:1214–1222. https://doi.org/10.1016/J.RSER.2014.10.092

Chakraborti D, Rahman MM, Ahamed S et al (2016) Arsenic groundwater contamination and its health effects in Patna district (capital of Bihar) in the middle Ganga plain, India. Chemosphere 152:520–529. https://doi.org/10.1016/J.CHEMOSPHERE.2016.02.119

Cheng W, Zhang W, Hu L, et al (2016) Etching synthesis of iron oxide nanoparticles for adsorption of arsenic from water †. https://doi.org/10.1039/c5ra26143k

Chenu S, Lebullenger R, Rocherullé J (2010) Characterization of NaPO3–SnO–WO3 glasses prepared by microwave heating. J Mater Sci 45:6505–6510. https://doi.org/10.1007/s10853-010-4739-2

Chiban M, Zerbet M, Carja G, Sinan F (2012) Application of low-cost adsorbents for arsenic removal: a review. J Environ Chem Ecotoxicol 4:91–102. https://doi.org/10.5897/JECE11.013

Chowdhury SR, Yanful EK, Pratt AR (2011) Arsenic removal from aqueous solutions by mixed magnetite–maghemite nanoparticles. Environ Earth Sci 64:411–423. https://doi.org/10.1007/s12665-010-0865-z

Debnath A, Deb K, Chattopadhyay KK, Saha B (2016a) Methyl orange adsorption onto simple chemical route synthesized crystalline α-Fe$_2$O$_3$ nanoparticles: kinetic, equilibrium isotherm, and neural network modeling. Desalin Water Treat 57:13549–13560. https://doi.org/10.1080/19443994.2015.1060540

Debnath A, Deb K, Das NS et al (2016b) Simple chemical route synthesis of Fe$_2$O$_3$ nanoparticles and its application for adsorptive removal of Congo red from aqueous media: artificial neural

network modeling. J Dispers Sci Technol 37:775–785. https://doi.org/10.1080/01932691.2015.1062772

Devi RR, Umlong IM, Das B et al (2014) Removal of iron and arsenic (III) from drinking water using iron oxide-coated sand and limestone. Appl Water Sci 4:175–182. https://doi.org/10.1007/s13201-013-0139-5

Dhar RK, Zheng Y, Rubenstone J, van Geen A (2004) A rapid colorimetric method for measuring arsenic concentrations in groundwater. Anal Chim Acta 526:203–209. https://doi.org/10.1016/J.ACA.2004.09.045

Fierro V, Muñiz G, Gonzalez-Sánchez G et al (2009) Arsenic removal by iron-doped activated carbons prepared by ferric chloride forced hydrolysis. J Hazard Mater 168:430–437. https://doi.org/10.1016/J.JHAZMAT.2009.02.055

Gallegos-Garcia M, Ramírez-Muñiz K, Song S (2012) Arsenic removal from water by adsorption using iron oxide minerals as adsorbents: a review. Miner Process Extr Metall Rev 33:301–315. https://doi.org/10.1080/08827508.2011.584219

Ghosal PS, Gupta AK (2016) Enhanced efficiency of ANN using nonlinear regression for modeling adsorptive removal of fluoride by calcined Ca–Al–(NO3)–LDH. J Mol Liq 222:564–570. https://doi.org/10.1016/J.MOLLIQ.2016.07.070

Ghosal PS, Gupta AK (2017) Development of a generalized adsorption isotherm model at solid-liquid interface: a novel approach. J Mol Liq 240:21–24. https://doi.org/10.1016/j.molliq.2017.05.042

Glocheux Y, Pasarín MM, Albadarin AB et al (2013) Removal of arsenic from groundwater by adsorption onto an acidified laterite by-product. Chem Eng J 228:565–574. https://doi.org/10.1016/J.CEJ.2013.05.043

Gu Z, Fang J, Deng B (2005) Preparation and evaluation of GAC-based iron-containing adsorbents for arsenic removal. Environ Sci Technol 39(10):3833–3843. https://doi.org/10.1021/es048179r

Hémono N, Chenu S, Lebullenger R et al (2010) Microwave synthesis and physical characterization of tin(II) phosphate glasses. J Mater Sci 45:2916–2920. https://doi.org/10.1007/s10853-010-4283-0

Herlekar M, Barve S, Kumar R (2014) Plant-mediated green synthesis of iron nanoparticles. J Nanoparticles 2014:1–9. https://doi.org/10.1155/2014/140614

Ibrahim HMM (2015) Green synthesis and characterization of silver nanoparticles using banana peel extract and their antimicrobial activity against representative microorganisms. J Radiat Res Appl Sci 8:265–275. https://doi.org/10.1016/J.JRRAS.2015.01.007

Jing H, Song H, Liang Z et al (2010) Equilibrium and thermodynamic parameters of adsorption of Methylene Blue onto rectorite. Fresenius Environ Bull 19:2651–2656

Kanel SR, Choi H (2017) Removal of Arsenic from groundwater by industrial byproducts and its comparison with zero-valent iron. J Hazard Toxic Radioact Waste 21:04016028. https://doi.org/10.1061/(ASCE)HZ.2153-5515.0000349

Li W-G, Gong X-J, Wang K, Zhang X-R, Fan W-B (2014) Adsorption characteristics of arsenic from micro-polluted water by an innovative coal-based mesoporous activated carbon. Bioresour. Technol. 165:166–173. https://doi.org/10.1016/J.BIORTECH.2014.02.069

Liu Z, Wan Y, Xiong G et al (2015) Three-dimensional porous nanocomposite of highly dispersed Fe_3O_4 nanoparticles on carbon nanofibers for high-performance microwave absorbents. Mater Express 5:113–120. https://doi.org/10.1166/mex.2015.1216

Mandal AK, Sen S, Mandal S et al (2015) Energy efficient melting of glass for nuclear waste immobilization using microwave radiation.

Int J Green Energy 12:1280–1287. https://doi.org/10.1080/15435075.2014.895735

Martínez-Cabanas M, López-García M, Barriada JL et al (2016) Green synthesis of iron oxide nanoparticles. Development of magnetic hybrid materials for efficient As(V) removal. Chem Eng J 301:83–91. https://doi.org/10.1016/J.CEJ.2016.04.149

Mercado-Borrayo BM, Schouwenaars R, Litter MI et al (2014) Metallurgical slag as an efficient and economical adsorbent of arsenic. Water Reclam Sustain. https://doi.org/10.1016/b978-0-12-411645-0.00005-5

Mishra PK, De V, Ghongane DE et al (2013) Preparation and characterisation of glass product with modified composition for vitrification of high level radioactive waste. J Therm Anal Calorim 112:103–108. https://doi.org/10.1007/s10973-012-2811-7

Mohan D, Pittman CU (2007) Arsenic removal from water/wastewater using adsorbents—a critical review. J Hazard Mater 142:1–53. https://doi.org/10.1016/J.JHAZMAT.2007.01.006

Mukherjee D, Ghosh S, Majumdar S, Annapurna K (2016) Green synthesis of α-Fe_2O_3 nanoparticles for arsenic(V) remediation with a novel aspect for sludge management. J Environ Chem Eng 4:639–650. https://doi.org/10.1016/J.JECE.2015.12.010

Popescu V, Batin MN, Popescu V (2011) Synthesis and characterization of iron oxide powders. Powder Metall Prog.11:201–205.

Ramrakhiani L, Halder A, Majumder A et al (2017) Industrial waste derived biosorbent for toxic metal remediation: mechanism studies and spent biosorbent management. Chem Eng J 308:1048–1064. https://doi.org/10.1016/J.CEJ.2016.09.145

Salameh Y, Albadarin AB, Allen S et al (2015) Arsenic(III, V) adsorption onto charred dolomite: charring optimization and batch studies. Chem Eng J 259:663–671. https://doi.org/10.1016/J.CEJ.2014.08.038

Smedley P, Kinniburgh D (2002) A review of the source, behaviour and distribution of arsenic in natural waters. Appl Geochem 17:517–568. https://doi.org/10.1016/S0883-2927(02)00018-5

Solé-Sardans M, Gamisans X, Dorado AD, Lao-Luque C (2016) Exploring arsenic adsorption at low concentration onto modified Leonardite. Water Air Soil Pollut 227:128. https://doi.org/10.1007/s11270-016-2827-x

Vu HT, Scarlett CJ, Vuong QV (2018) Phenolic compounds within banana peel and their potential uses: a review. J Funct Foods 40:238–248. https://doi.org/10.1016/J.JFF.2017.11.006

Weng C-H, Lin D-F, Chiang P-C (2003) Utilization of sludge as brick materials. Adv Environ Res 7:679–685. https://doi.org/10.1016/S1093-0191(02)00037-0

Willis AL, Turro NJ, O'Brien S (2005) Spectroscopic Characterization of the Surface of Iron Oxide Nanocrystals. Chem. Mater. 17:5970–5975. https://doi.org/10.1021/CM051370V

Yu J, Xiong W, Zhu J et al (2017) Removal of Congo red from aqueous solution by adsorption onto different amine compounds modified sugarcane bagasse. Clean Technol Environ Policy 19:517–525. https://doi.org/10.1007/s10098-016-1243-7